Available online at www.sciencedirect.com

SCIENCE DIRECT

Materials Letters 59 (2005) 2026–2031

materials letters

www.elsevier.com/locate/matlet

Electrochemical characterization of sol–gel hybrid coatings in cobalt-based alloys for orthopaedic implants

L.E. Amato, D.A. López, P.G. Galliano, S.M. Ceré*

INTEMA, Universidad Nacional de Mar del Plata, Conicet, Juan B. Justo 4302, Mar del Plata B7608FDQ, Argentina

Received 15 June 2004; accepted 16 February 2005
Available online 17 March 2005

Abstract

Cobalt-based alloys are widely used for the fabrication of several devices that are surgically implanted in the body due to their good corrosion and wear resistance as well as their good biocompatibility. However, the carcinogenic potential of metal elements used in total hip arthoplasty components is a concern. This work describes the development of hybrid coatings containing methyltriethoxysilane (MTES) and tetraethylorthosilicate (TEOS) acidic sol, applied by the dip coating method onto ASTM F75 alloys sintered at 450 °C and 550 °C. The performance of the coated metal was evaluated in vitro by classical electrochemical techniques and compared to the uncoated material.

Keywords: Thin films; Coatings; Sol–gel; Corrosion; Cobalt-based alloys

1. Introduction

In situ degradation of orthopaedic implants is a highly undesirable process affecting not only the integrity of the prosthesis but producing a systemic response to the body. There is a long clinical experience with temporary and permanent metal implants, with the biocompatibility of such implants regarding local tissue reaction being a major concern. Although materials that are commonly used for orthopaedic devices are characterized by their high corrosion resistance in body fluid, there are many studies that have shown an important increase of metal ions in implants' surrounding tissues [1,2]. Clinical studies on Co–Cr–Mo alloys showed the presence of chromium orthophosphate in the implant's surrounding tissues and it has been demonstrated that this chemical compound is able to stimulate osseous resorption and necrosis of the periprosthetic tissue [3,4]. One way of minimizing the oxidation of the metal is by applying a protective coating on the metal surface. Inorganic coatings with vitreous structure have been widely used as protective coatings for metals and alloys, tending to improve the chemical and physical properties of the metallic substrate surfaces [5]. Gallardo et al. had reported that hybrid sol–gel coatings applied on 316L stainless steel inhibited corrosion and diffusion of Fe ions, although no signs of bioactivity were detected [6]. Only coating obtained with suspensions prepared by adding either glass or glass–ceramic particles showed bioactivity [7,8].

This work presents the electrochemical performance of a silica-based coating applied by the sol–gel method on Co–Cr–Mo alloys (ASTM F75) as-cast in simulated body fluid (SBF). The coating contains Si–CH_3 groups resulting in a hybrid organic–inorganic layer.

2. Experimental

Rectangular planar samples with an area of 2 cm^2 of ASTM F75 alloys were cut from a bar obtained from Korb

Table 1
Chemical composition of ASTM F75 alloys (wt.%)

Cr	Mo	Ni	Fe	C	Si	Mn	Co
27.0–30.00	5.0–7.00	≤1.00	≤0.75	≤0.35	≤1.00	≤1.00	Balance

* Corresponding author. Tel.: +54 223 481 6600; fax: +54 223 4810046.
E-mail address: smcere@fi.mdp.edu.ar (S.M. Ceré).

0167-577X/$ - see front matter © 2005 Elsevier B.V. All rights reserved.
doi:10.1016/j.matlet.2005.02.010

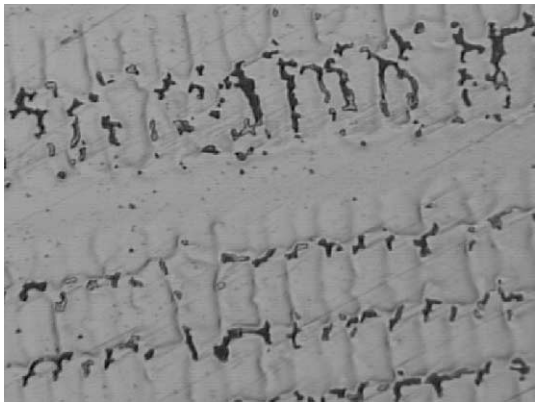

Fig. 1. Microstructure of the as-cast F75 alloys (200×).

and Olson. The chemical composition of the alloy is presented in Table 1 [9].

Samples were polished with emery paper and alumina (0.3 μm) until mirror finish. In order to analyse the resulting microstructure, some samples were etched by applying 3.5 V for 10 min in HCl 2% p/v before they were microscopically observed [10].

Sol–gel coatings were obtained by dipping the substrates in the silica colloidal dispersion (sol) made from the hydrolysis and polycondensation of tetraethylorthosilicate (TEOS) and methyltriethoxysilane (MTES) in a ratio of 40:60 in moles. Acetic acid was used as catalyser and disperser, and ethanol was employed as solvent. The synthesis was made at 40 °C under reflux during 3 h. Density and viscosity were measured at the end of the process. A detailed preparation process is described elsewhere [11].

Polished samples were preoxidised for 30 min at 300 °C in an electric oven, cooled in air, and then ultrasonically cleaned and dipped in isopropylic alcohol in order to enhance coating adherence. Afterwards, they were dipped in the sol and withdrawn at 3.5 cm s^{-1}. The samples were dried for 2 h in air and then were treated either at 450 °C or 550 °C for 30 min in an electric oven.

Scanning electron microscopy (SEM) and optical microscopy (Olympus S041) were used to study the structural integrity of the coating. Electrochemical tests

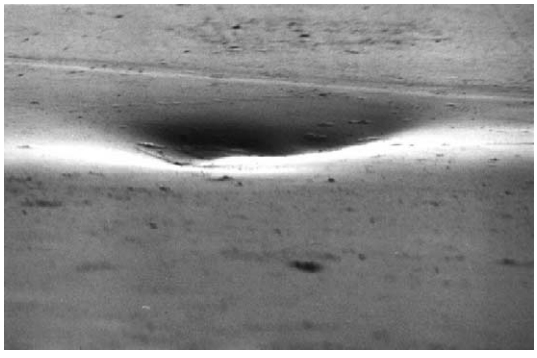

Fig. 2. SEM micrograph of the coated samples sintered at 450 °C (1000×).

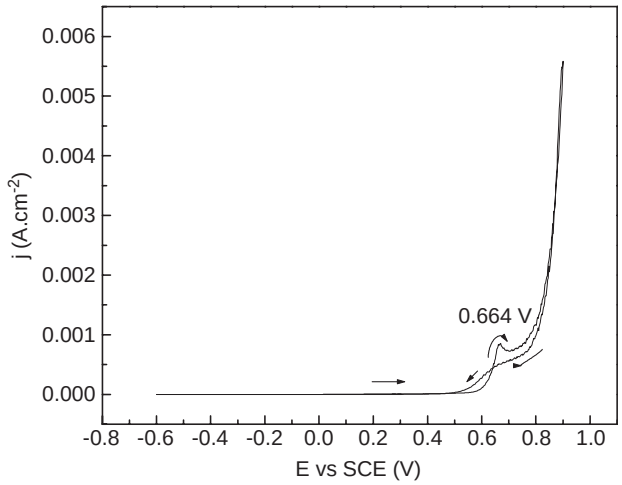

Fig. 3. Voltammogram of ASTM F75 alloys in SBF.

were conducted in SBF solution [12] at 37 °C, pH 7.3±0.1, prepared with bidistilled water grade I (Millipore). Coated samples were included in polyester resin and an appropriated electrical contact was made through a brass rod with silver epoxy resin in the back of the sample both to ensure electrical continuity and serve as sample holder. Electrochemical experiments were performed using a Gamry CMS 100 electrochemical unit. A conventional three-electrode cell was used with a saturated calomel electrode (SCE, Radiometer Copenhagen) as reference electrode and a platinum wire of convenient area as counter electrode.

Potentiodynamic polarization curves were conducted from −0.6 V to 0.9 V at a sweep rate of 0.002 V s^{-1}. Electrochemical impedance spectroscopy (EIS) experiments were registered at the corrosion potential (E_{cor}) with an amplitude of 0.005 V rms, sweeping frequencies from

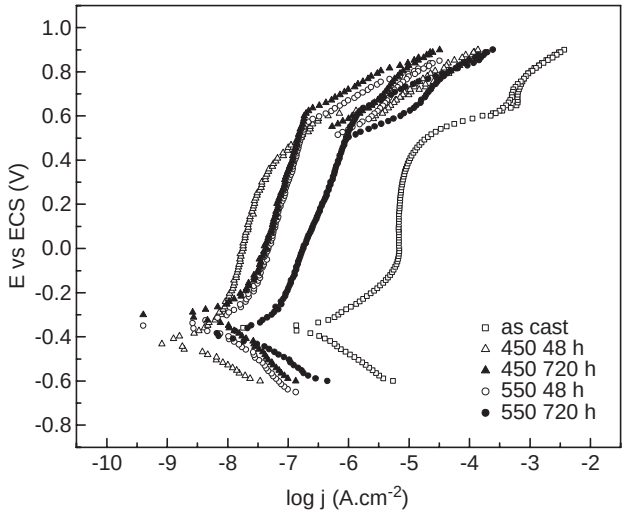

Fig. 4. Potentiodynamic polarisation curves for Co–Cr–Mo alloys without and with coating sintered at either 450 °C or 550 °C (48 and 720 h of immersion).

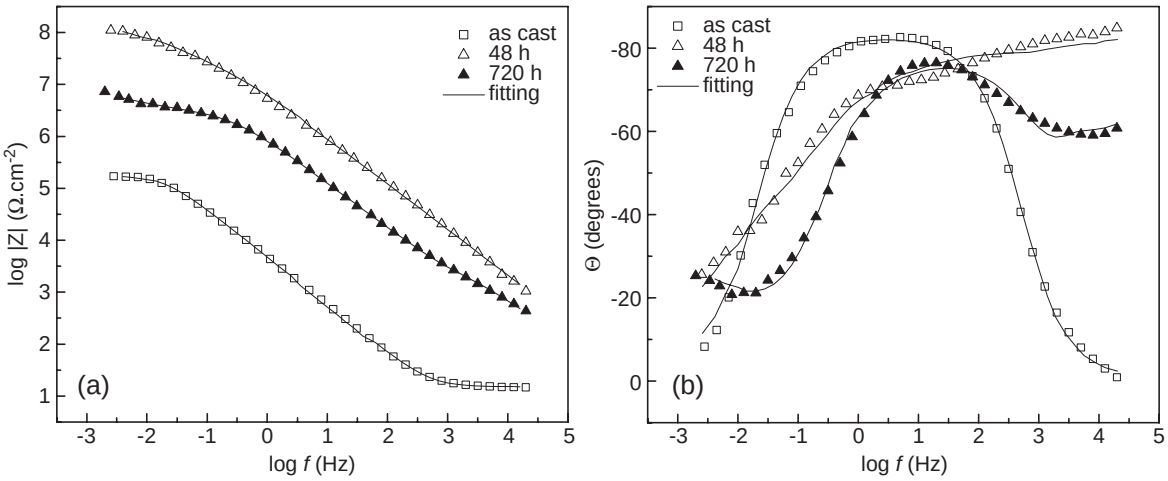

Fig. 5. EIS Bode diagrams for Co–Cr–Mo alloy without (1 h) and with coating sintered at 450 °C (48 and 720 h of immersion). (a) $|Z|$ vs. $\log f$. (b) θ vs. $\log f$.

20,000 to 0.003 Hz. Impedance data fitting was performed using Zplot software [13].

3. Results and discussion

Fig. 1 shows the microstructure of the as-cast F75 alloy. A typical solidification structure consisting of a highly segregated dendritic structure where chromium-rich carbides are dispersed in the dendritic matrix can be observed [9].

Fig. 2 shows a SEM photograph of a coated sample sintered at 450 °C. Similar results were obtained at 550 °C. It can be observed that the hybrid coating is able to adapt itself to substrate singularities and the coating is continuous and free of defects.

The electrochemical behaviour of the substrate was characterised by a voltammogram (Fig. 3). It can be seen that the alloy remained in the passive state from −0.6 to 0.6 V, and that the current density registered was very low, indicating no faradaic processes occurring in this potential range. The anodic peak around 0.7 V is related to the conversion of the passive film into a higher valence form, presumably related to Cr(IV) species in the form of CrO_4^{2-}. Further anodic polarisation leads to simultaneous formation of CrO_4^{2-} species and oxygen evolution. There is no evidence of reduction peaks, suggesting that the film formed on the chromium alloys is not easily removed by cathodic reduction in the electrolyte and/or the surface is immediately passivated after immersion in the electrolyte and remains in such state until transpassive potential is achieved [14,15].

Fig. 4 presents potentiodynamic polarisation curves for Co–Cr–Mo alloy with and without coating sintered at either 450 °C or 550 °C, for two immersion times. It can be observed that all the coated samples showed a lower passivation current density than the uncoated samples. On the other hand, the coating does not change either the potential breakdown or the protection potential for any of the studied samples. After 720 h of immersion in SBF, the protective properties seem to diminish, with an increase of the passivation current density for both kinds of coatings. This can be attributed to the attack of the alloy due to pores

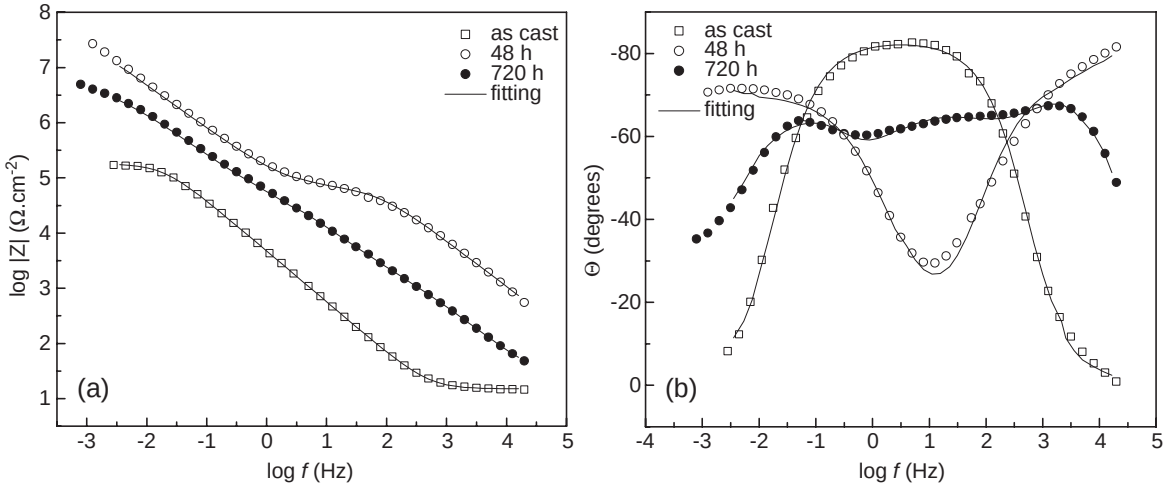

Fig. 6. EIS Bode diagrams for Co–Cr–Mo alloy without and with coating sintered at 550 °C (48 and 720 h of immersion). (a) $|Z|$ vs. $\log f$. (b) θ vs. $\log f$.

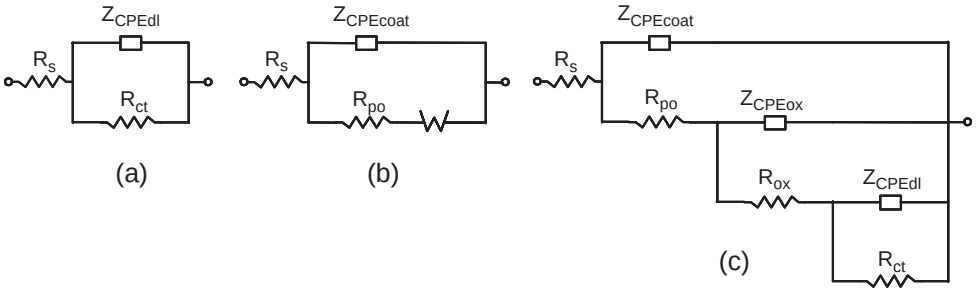

Fig. 7. Equivalent electric circuits employed to model the impedance data. (a) As-cast alloy; (b) coated alloys, 48 h; (c) coated alloys, 720 h.

or imperfections on the coating, leading to a localized attack that produces greater areas of contact between the alloy and the solution. Coatings sintered at 450 °C showed a better performance than the ones at 550 °C, which presented higher passivation current densities compared to the first ones.

Impedance measurements were made during 30 days with intervals of 24–48 h in order to observe the system response with time. Figs. 5 and 6 show EIS Bode diagrams for the as-cast Co–Cr–Mo alloy and the coated alloy sintered at 450 °C and 550 °C at two different immersion times (48 and 720 h). The full line represents fitted values based on the corresponding equivalent electric circuits.

The impedance diagrams for the uncoated substrate present a sole time constant evidenced in the Bode phase plot by the presence of a maximum between 10^{-2} and 5×10^{2} Hz. The change in the impedance response suggests a nonideal dielectric capacitive behaviour, which can be modelled by a Randles circuit with a constant phase element or CPE (Fig. 7a). A CPE can be described by the expression:

$$Z_{\mathrm{CPE}} = \frac{1}{Y_0(j\omega)^n} \tag{1}$$

with $-1<n<1$ [16]. In this equation, n is a coefficient associated with system homogeneity (being 1 for an ideal capacitor), ω is the frequency, and Y_0 is the pseudocapacitance of the system. The corresponding fitted parameters are shown in Table 2.

According to the impedance diagrams, the coated samples results can be analyzed separately by considering their immersion times. Sol–gel coatings used as protection of different metals against corrosion do not always improve with the immersion time. In fact, depending on the composition and structure of the coating (totally inorganic or hybrid), the electrolytic medium, and the soaking time, deterioration of the coatings occurs, permitting the contact of the electrolyte with the substrate and thus decreasing the protective effect [18]. However, the application of sol–gel coatings usually leads to an improvement in the corrosion protection with respect to the uncoated base material.

After 48 h of immersion, the impedance data of either the samples sintered at 450 °C or 550 °C can be modelled by a Warburg-type diffusion component in the EIS spectrum that can be attributed to diffusion processes taking place in the solid phase. This suggests the presence of pores in the outer part of the coating with diffusion effects inside them [17]. The Warburg impedance is used to model increasing ionic conductivity due to corrosion process occurring into the pores and increasing diffusivity into the pores. It can be described by the equation [13]:

$$Z_{\mathrm{w}} = \frac{R_{\mathrm{DO}}}{(jT\omega)^{n_{\mathrm{d}}}}\tanh(jT\omega)^{n_{\mathrm{d}}} \tag{2}$$

where R_{DO} is associated with the solid phase diffusion and T is related to the diffusion coefficient and pore length.

The spectra are properly fitted by a circuit that includes a Warburg element (Fig. 7b). The corresponding fitting results are given in Table 3.

The values of R_{po}, related to the diffusion through the pores of the coating, are higher for the samples sintered at 450 °C than those treated at 550 °C, indicating the presence of smaller pores for the first kind of samples. Correspondingly, the values of pseudocapacitance ($Y_{0\ \mathrm{coat}}$) are lower. An increase in the $Y_{0\ \mathrm{coat}}$ value can be attributed to the increase in the exposure area due to delamination, water uptake into the pores, and/or corrosion, thus a lower value can be associated with a coating with better insulation

Table 2
Circuit parameters for the as-cast alloy at 1 h of immersion

	As-cast alloy
R_{s} (Ω cm^2)	15±0.05
$Y_{0\ \mathrm{dl}}$ (Ω^{-1} cm^{-2} s^n)	$3.86\times10^{-5}\pm1.06\times10^{-7}$
n	0.92 ± 6.1910^{-4}
R_{ct} (Ω cm^2)	$1.81\times10^{5}\pm890.52$

Table 3
Circuit parameters for the coated alloys sintered at 450 °C and 550 °C at 48 h of immersion

	450 °C	550 °C
R_{s} (Ω cm^2)	15±0.05	15±0.05
$Y_{0\ \mathrm{coat}}$ (Ω^{-1} cm^{-2} s^n)	$2.75\times10^{-8}\pm5.07\times10^{-10}$	$9.32\times10^{-8}\pm2.66\times10^{-9}$
n_{coat}	$0.88\pm2.27\times10^{-3}$	$0.83\pm2.27\times10^{-3}$
R_{po} (Ω cm^2)	$7.02\times10^{5}\pm1.03\times10^{3}$	$7.32\times10^{4}\pm0.91\times10^{3}$
R_{DO} (Ω cm^2)	$1.57\times10^{8}\pm6.49\times10^{6}$	$6.98\times10^{7}\pm3.54\times10^{6}$
n_{D}	$0.34\pm8.21\times10^{-3}$	$0.78\pm2.51\times10^{-3}$
T	90.39±4.82	420.10±25.69

Table 4
Circuit parameters for the coated alloys sintered at 450 °C and 550 °C at 720 h of immersion

	450 °C	550 °C
R_s (Ω cm^2)	25±0.92	25±0.87
$Y_{0\ coat}$ (Ω^{-1} cm^{-2} s^n)	$1.25\times10^{-7}\pm1.69\times10^{-8}$	$1.03\times10^{-6}\pm2.83\times10^{-8}$
n_{coat}	$0.85\pm1.14\times10^{-2}$	$0.87\pm2.55\times10^{-3}$
R_{po} (Ω cm^2)	4266±446.85	2239±112.58
$Y_{0\ ox}$ (Ω^{-1} cm^{-2} s^n)	$1.01\times10^{-7}\pm1.58\times10^{-8}$	$2.66\times10^{-6}\pm8.01\times10^{-8}$
n_{ox}	$0.87\pm1.36\times10^{-2}$	$0.68\pm4.63\times10^{-3}$
R_{ox} (Ω cm^2)	$2.74\times10^{6}\pm7.04\times10^{4}$	$2.54\times10^{5}\pm2.36\times10^{4}$
$Y_{0\ dl}$ (Ω^{-1} cm^{-2} s^n)	$1.54\times10^{-6}\pm1.08\times10^{-7}$	$1.35\times10^{-6}\pm7.96\times10^{-8}$
n	$0.44\pm1.54\times10^{-2}$	$0.88\pm2.31\times10^{-2}$
R_{ct} (Ω cm^2)	$1.01\times10^{20}\pm2.35\times10^{13}$	$6.23\times10^{6}\pm1.42\times10^{5}$

properties [19]. On the other hand, the samples sintered at 450 °C present higher resistance to solid phase diffusion (R_{DO}) and lower values of T, related to the porous length [20]. These results could be associated with the presence of a coating with superior protective properties at short immersion times in SBF when the sintering process is conducted at 450 °C.

While the immersion time increases up to 720 h, the coating protective properties decrease as the coating degrades in the samples sintered both at 450 °C and 550 °C. The impedance diagrams can thus be modelled by an equivalent circuit considering a multilayer system (Fig. 7c), which takes into account the presence of a superficial oxide that is formed on the metal substrate when the electrolyte reaches the pore base. The fitted parameters are shown in Table 4.

According to this equivalent circuit, three-time constants should be observed in the corresponding impedance diagrams, associated with the coating, the oxide, and the charge transfer processes, respectively. However, this is not the case for the samples sintered at 450 °C. This could be explained by considering that, despite the degradation process that undertakes the coating, this is not as severe as that of the samples treated at 550 °C. Therefore, the time constant associated with the charge transfer in the metal appears at very low frequencies ($\tau \cong 10^{-14}$ Hz), out of range of the scale of the diagram. This is supported by the higher values of R_{po} and the lower values of $Y_{0\ coat}$ registered in the samples sintered at 450 °C with respect to the ones sintered at 550 °C. The first is correlated with the presence of small pores in the coating, while the lower pseudocapacitance is related to a minor active area exposed. Moreover, the values of R_{ox} and $Y_{0\ ox}$ follow the same trend and are consistent with these asseverations as can be seen in Table 4.

The better performance of the coated samples sintered at 450 °C observed in the impedance results at both short and long immersion times is in agreement with the results obtained by the potentiodynamic polarisation curves (Fig. 4). This could be related to a higher concentration of methyl groups in the surface of the samples treated at 450 °C, which retains the hybrid structure of the coating [21]. The hydrophobic nature of these methyl groups restricts the access of the aqueous electrolyte into the coating pores, thus enhancing the resistance of the coated material.

4. Conclusions

Hybrid inorganic–organic coatings on Co–Cr–Mo alloy ASTM F75 were obtained using methyltriethoxysilane (MTES) and tetraethylorthosilicate (TEOS) acidic sol. The dip coating method led to the formation of a continuous and defect-free layer, when it was sintered either at 450 °C or 550 °C.

The electrochemical properties of the system demonstrated that the protective behaviour of the coating was superior for the samples sintered at 450 °C with respect to the ones treated at 550 °C. This could be associated with a higher concentration of methyl groups in the surface of the first kind of samples, retaining the hybrid structure of the coating. The presence of these methyl groups generates a hydrophobic barrier that restricts the access of the aqueous electrolyte into the coating pores, improving the corrosion resistance of the coated material.

Acknowledgments

This work has been partially financed by the Cyted project VIII.9, the TWAS research grant R6/CHE/LA 01-216, and the PICTO grant 11338. The authors are grateful to Dra. Susana Rosso for her valuable assistance and helpful comments during the revision of this paper.

References

[1] H. Agins, N. Akock, M. Bansal, E. Salvati, P. Wilson, P. Pellici, P. Bullough, J. Bone Jt. Surg. 71A (1988) 347.
[2] J. Jacobs, J. Gilbert, R. Urban, J. Bone Jt. Surg. 80 (1998) 268.
[3] S. Lee, F. Brennan, J. Jacobs, P. Urban, D. Ragusa, T. Glant, J. Orthop. Res. 15 (1997) 40.
[4] E. Mathiensen, J. Lind Gren, G. Blongrem, F. Reinholt, J. Bone Jt. Surg. 73B (1991) 569.
[5] P. de Lima Nieto, M. Atik, L.A. Avaca, M. Aegerter, J. Sol-Gel Sci. Technol. 2 (1994) 529.
[6] J. Gallardo, P. Galliano, A. Durán, J. Sol-Gel Sci. Technol. 21 (2001) 65.
[7] A. Durán, A. Conde, A. Gómez Coedo, T. Dorado, C. García, S. Ceré, J. Mater. Chem. 14 (2004) 1.
[8] J. Ballarre, J.C. Orellano, C. Bordenave, P. Galliano, S. Ceré, J. Non-Cryst. Solids 304 (2002) 278.
[9] L. Korb, D. Olson, Metals Handbook, 9th edition, Corrosion, vol. 13, ASM International, Metals Park, Ohio, 1987.
[10] H. Plako, S. Brown, J. Payer, J. Biomed. Mater. Res. 39 (1998) 292.
[11] J. Gallardo, Ph.D. thesis, University of Mar del Plata, Mar del Plata (1999).

[12] T. Kokubo, H. Kushitani, S. Sakka, T. Kitsugi, T. Yamamuro, J. Biomed. Mater. Res. 14 (1990) 721.
[13] Zplot for Windows, Electrochem. Impedance Software Operating Manual, Part 1, Scribner Ass., Inc., Southern Pines, NC, 1998.
[14] M. Metikos-Hukovic, S. Omanovic, R. Babic, I. Milosev, Ber. Bunsenges. Phys. Chem. 98 (10) (1994) 1243.
[15] C.A. Melendres, M. Pankuch, Y.S. Li, R.L. Knight, Electrochim. Acta 37 (15) (1992) 2742.
[16] CMS100 Sytems, Operator's Manual Addendum. Changes for CE Compliance, Gamry Instruments, Inc., PA, USA, 1996.
[17] M. Metikos-Hukovic, E. Tkalcec, A. Kwokal, J. Piljac, Surf. Coat. Technol. 165-1 (2003) 40.
[18] A. Pepe, M. Aparicio, S. Ceré, A. Durán, Preparation and characterisation of cerium doped silica sol–gel coatings on glass and aluminium substrates, J. Non-Cryst. Solids 348 (2004) 162–171.
[19] F. Mansfeld, J. Appl. Electrochem. 25 (1995) 187.
[20] C. Liu, Q. Bi, A. Leyland, A. Matthews, Corros. Sci. 45 (2003) 1257.
[21] J. Gallardo, A. Durán, D. Di Martino, R.M. Almeida, J. Non-Cryst. Solids 298 (2002) 219.